

# Insight into the Loading and Release Properties of an Exfoliated Kaolinite/Cellulose Fiber (EXK/CF) Composite as a Carrier for Oxaliplatin Drug: Cytotoxicity and Release Kinetics

Lijun Tian, Mostafa R. Abukhadra,\* Aya S. Mohamed, Ahmed Nadeem, Sheikh F. Ahmad, and Khalid E. Ibrahim



Cite This: *ACS Omega* 2020, 5, 19165–19173



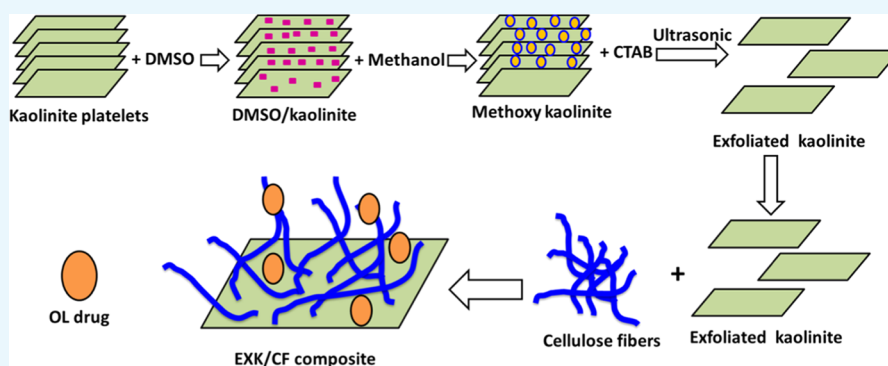
Read Online

ACCESS |

Metrics & More

Article Recommendations

Supporting Information



**ABSTRACT:** Kaolinite layers were exfoliated as single sheets and admixed with cellulose fibers, forming an advanced exfoliated kaolinite/cellulose fiber (EXK/CF) composite, which was characterized as a promising carrier for the oxaliplatin (OL) drug to induce safety as well as the therapeutic effect. The EXK/CF composite exhibited promising loading capacity and achieved an experimental value of 670 mg/g and an expected theoretical value of 704.4 mg/g. The loading behavior of OL using the EXK/CF composite followed the pseudo-first-order kinetic model and the Langmuir equilibrium model, achieving an adsorption energy of 7.7 kJ/mol. This suggested physisorption and homogeneous loading behavior of the OL molecules in a monolayer form. The release profile of OL from EXK/CF continued for about 100 h with maximum release percentages of 86.4 and 95.2% in the phosphate and acetate buffers, respectively. The determined diffusion exponent from the Korsmeyer–Peppas kinetic model suggested non-Fickian transport behavior of the OL molecules and releasing behavior controlled by erosion as well as diffusion mechanisms. Regarding the cytotoxic effect, the EXK/CF composite has a high safety impact on the normal colorectal cells (CCD-18Co) and higher toxic impacts on the colorectal cancer cell (HCT116) than the free oxaliplatin drug.

## 1. INTRODUCTION

Oxaliplatin (OL) as a chemotherapy drug for colorectal cancer was recommended and approved by the Food and Drug Administration as an effective drug for the cancer cells at the different stages of the disease.<sup>1,2</sup> Unfortunately, there are some drawbacks that reduce the safety value of oxaliplatin as it is normally associated with significant side effects including cardiotoxicity, myelotoxicity, chronic peripheral neuropathy, nausea, and gastrointestinal (GI) tract disorders.<sup>1,3,4</sup> Moreover, it is like most of the traditional therapies as it shows low solubility properties, narrow therapeutic window, and poor distribution patterns. The previous drawbacks are of strong influence in reducing its effect on the cancer cells and having toxic impact on the normal cells, which set several considerations for its dosages to be applied.<sup>5</sup>

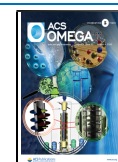
Development of suitable carriers for the target drug molecules was recommended as an advanced method to

control the release profiles of the drugs and induce their safety properties to overcome the commonly reported side effects.<sup>6,7</sup> Additionally, the advanced types of drug carriers have a vital role in (a) reducing the drug degradation rates, (b) accelerating their solubility, (c) controlling the drug diffusion rates according to the acceptable therapeutic levels, (d) enhancing their selectivity properties toward the cancer cells, and (e) enhancing their pharmacological and curative profiles.<sup>6,8</sup> Several materials were studied as delivery systems for the oxaliplatin drug to reduce its toxic effects and induce its

Received: May 28, 2020

Accepted: July 15, 2020

Published: July 23, 2020



therapeutic performance including the mesoporous silica, types of polymers, liposomes, alginate nanogels, and lipid nanoparticles. All of these carriers were used to promote the permeation as well as the retention properties of the oxaliplatin drug.<sup>5,9,10</sup>

It was expected that a hybrid structure developed from clay minerals and natural biopolymers will be an effective carrier for cancer chemotherapy drugs and might be of vital role in inducing the therapeutic as well as the safety properties of oxaliplatin.<sup>8</sup> Clay minerals include several species of layered silicate minerals, and all of them have significant surface area, high natural reserves, low cost, excellent adsorption properties, nontoxicity, high biocompatibility values, and significant ion exchange properties.<sup>11,12</sup> Kaolinite and montmorillonite are the most studied clay minerals in industrial and medical applications.<sup>13</sup> Kaolinite is a hydrous form of aluminum silicate clay minerals of a 1:1 layered structure.<sup>11</sup> Although the kaolinite mineral has higher availability and lower cost than the other clay minerals like montmorillonite, its application as a drug carrier is very limited. This might be related to its lower surface area, lower loading capacity, higher releasing rate, and lower ion exchange capacities than those of the other clay minerals of bentonite and halloysite.<sup>13</sup>

Modification of kaolinite by organic as well as inorganic reagents was suggested to enhance its qualification as a drug delivery system either by simple surface modifications or by intercalation of its layered structures with polymer chains.<sup>11,14</sup> Recently, the exfoliation of the clay layers as single sheets was suggested as an advanced modification technique, which resulted in a stunning enhancement in the surface reactivity, surface area, and adsorption capacities of the clay minerals.<sup>15,16</sup> Several studies were introduced for the exfoliation of montmorillonite, but unfortunately, little work focused on the production of exfoliated kaolinite sheets.<sup>15,16</sup> To the best of our knowledge, no previous work has evaluated the kaolinite separated sheets for the medical, industrial, and environmental applications either as a pure phase or as a composite with other materials.

The integration between kaolinite exfoliated sheets and cellulose fibers as natural biopolymers might result in an advanced composite of promising properties as a drug delivery system including biodegradability, biocompatibility, and surface reactivity.<sup>16</sup> Cellulose is a natural biopolymer of polysaccharide type and is having wide environmental, medical, and industrial applications.<sup>17</sup> Structurally, it is composed of two rings of anhydroglucose that connect with each other by types of  $\beta$ -1,4-glycosidic bonds. Technically, the cellulose-based materials are of high reactivity, high surface area, high stability, high biocompatibility value, high safety and nontoxicity properties, and high biodegradability.<sup>18,19</sup>

Based on the previous considerations, the introduced study involved the synthesis of a novel exfoliated kaolinite sheet/cellulose fiber (EXK/CF) composite and its characterization as a carrier for the oxaliplatin drug with enhanced loading capacity, release properties, and safety properties. The study involved estimation of the loading and releasing properties of the carrier and the main mechanisms that controlled the reactions based on different kinetic and equilibrium models. Additionally, the cytotoxicity properties of the EXK/CF composite were addressed for the cancer cells as well as the normal cells.

## 2. RESULTS AND DISCUSSION

**2.1. Characterization of the Carriers.** **2.1.1. X-ray Diffraction (XRD) Analysis.** The used kaolinite mineral was identified by its main diffraction peaks at about 12.33, 20.85, 24.87, and 26.64° that were assigned to the (001), ( $\bar{1}10$ ), (002), and (111) crystallographic planes of the triclinic crystal system, respectively, and its *d*-spacing was estimated to be 0.72 nm (Figure 1A). The intercalation of kaolinite sheets with

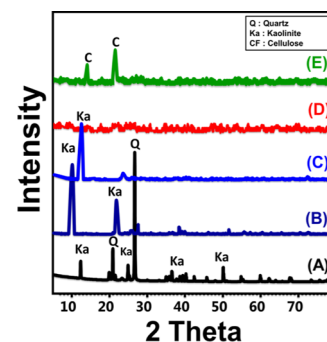


**Figure 1.** XRD patterns of raw kaolinite (A), DMSO-intercalated kaolinite (B), methoxy kaolinite (C), exfoliated kaolinite (EXK) (D), and the exfoliated kaolinite/cellulose fiber (EXK/CF) composite (E).

dimethyl sulfoxide (DMSO) molecules resulted in a diffraction pattern of significant broad peaks related to crystalline kaolinite ((001) and (002)). These two peaks were detected as broad peaks of deviated positions and of significantly high *d*-spacing (1.2 nm) (Figure 1B). The reported expansion between the main layered units of kaolinite was related to the expected destruction of the binding hydrogen bonds between them by DMSO. The obtained sample after the modification of kaolinite by methanol displayed a diffraction pattern close to that obtained for DMSO/kaolinite with observable declination in their intensities, noticeable shifting from their positions, and reduction in the *d*-spacing to be 0.92 nm (Figure 1C). The recognized pattern of the kaolinite sample after the final exfoliation step appeared as a smooth peak with no significant detection of kaolinite-related peaks, demonstrating destruction of the lattice structure and separating the units as individual sheets (Figure 1D). The combination between the exfoliated kaolinite sheets and the cellulose fiber was reflected in the diffraction pattern as it showed two noticeable peaks at about 14.91 and 22.72° that were related to crystalline cellulose fibers, confirming the integration between them in the composite (EXK/CF) (Figure 1E).

**2.1.2. Morphological Studies.** The scanning electron microscopy (SEM) image of the used kaolinite showed well-crystalline flakey grains with their distinguished pseudo-hexagonal morphology (Figure 2A). This was also confirmed by the high-resolution transmission electron microscopy (HRTEM) image of the sample, where the flakey kaolinite grains appeared with their pseudo-hexagonal morphology but exhibiting stacking above each other in a layered form (Figure 2B). The exfoliation of the kaolinite layers was followed at different stages, and the exfoliation process resulted in stripping of the layers into individual sheets with observable curvature of their edges as an initial stage for their scrolling under the organic expansion reactions (Figure 2C). Other images reflected the presence of kaolinite as a single pseudo-hexagonal layer of kaolinite with partial smoothing of the edges under the exfoliation effects (Figure 2D). The

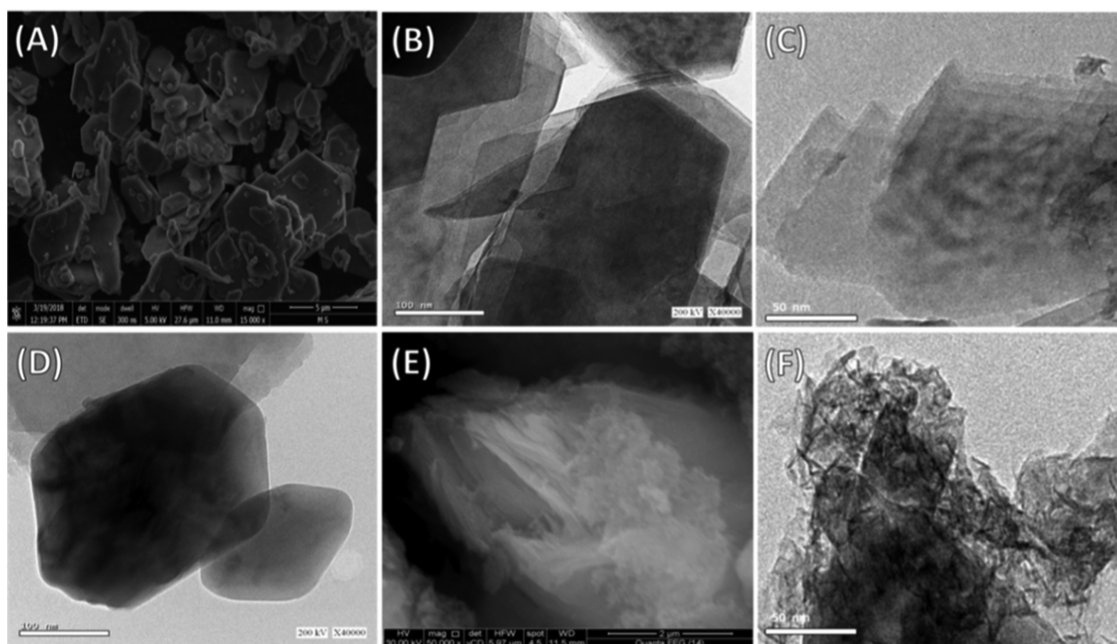


**Figure 2.** SEM image of raw kaolinite (A), HRTEM image of the raw kaolinite (B), HRTEM image of the exfoliated kaolinite layer with curvature of the edges (C), HRTEM image of exfoliated kaolinite flakes with pseudo-hexagonal morphology (D), the SEM image of the exfoliated kaolinite/cellulose fiber (EXK/CF) composite (E), and the HRTEM image of the exfoliated kaolinite/cellulose fiber (EXK/CF) composite (F).

integration between the exfoliated kaolinite sheets and the cellulose fibers was inspected by both the SEM and the HRTEM images (Figure 3E,F). In the SEM image, the

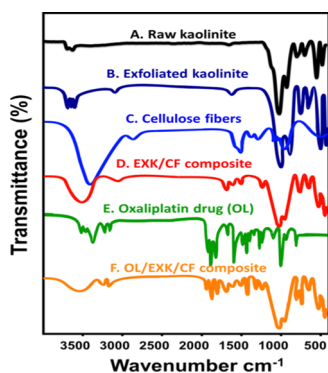


**Figure 3.** Fourier transform infrared (FT-IR) spectra of raw kaolinite (A), exfoliated kaolinite (B), cellulose fibers (C), the synthetic EXK/CF composite (D), the oxaliplatin (OL) drug (E), and the EXK/CF composite after its loading with the OL drug molecules.

exfoliated kaolinite layers appeared to be coated by nano-cellulose fibers (Figure 2E). This was supported by the HRTEM image that showed the kaolinite layer enclosed with bloom from cellulose nanofibers with different orientations (Figure 2F). Such integration processes and the associated changes in the morphologies reflected in the textural properties of the composite, especially the surface area. The measured surface areas of kaolinite, exfoliated kaolinite, and the EXK/CF composite were 10, 80.2, and 104 m<sup>2</sup>/g, respectively.

**2.1.3. FT-IR Analysis.** The essential functional groups of kaolinite were identified in the raw sample, and the detected groups are the Si–OH group (3689 cm<sup>-1</sup>), Al–OH (3500 and 912 cm<sup>-1</sup>), O–H bending (1641 cm<sup>-1</sup>), Si–O–Si (1020 cm<sup>-1</sup>), Si–O group (787 and 456 cm<sup>-1</sup>), and Si–O–Al (680 and 526 cm<sup>-1</sup>)<sup>11</sup> (Figure 3A). The exfoliated kaolinite sheets

show the same bands as those of raw kaolinite but with considerable deviation for the absorption bands, suggesting the distortion of silica tetrahedron units as well as the aluminum octahedron units during the exfoliation process<sup>13</sup> (Figure 3B). The spectrum of the cellulose fibers demonstrated the presence of the characteristic structural groups: –O–H stretching (3450 cm<sup>-1</sup>), adsorbed water (1640 cm<sup>-1</sup>), –C–H groups (1367 and 2914 cm<sup>-1</sup>), –C–O–C pyranose rings (1057 cm<sup>-1</sup>), and the  $\beta$ -glycosidic linkages (897 cm<sup>-1</sup>)<sup>21</sup> (Figure 3C).

The recognized spectrum of the EXK/CF composite emphasized the existence of complex absorption bands related to both the kaolinite essential groups and the cellulose structural groups (Figure 3D). This confirmed the integration between them in the composite with observable detection of the bands related to the –C–H, –C–O–C, and  $\beta$ -glycosidic linkages (Figure 3D). The integration effect was also observed with considerable shifting of the essential bands of exfoliated kaolinite as well as the cellulose fibers. The spectrum of the EXK/CF composite after loading it with the OL drug (Figure 3F) was studied in comparison with the spectrum of the OL drug to confirm the loading process (Figure 3E). The recognized bands emphasized the existence of the previously detected structural groups of the EXK/CF composite in addition to other new bands related to the characteristic groups of the OL drug (Figure 3F). The principal groups of the OL drug that were detected were the Pt bond at about 550 cm<sup>-1</sup>, N–H bending at 864.3 cm<sup>-1</sup>, and C=O bending at about 1562.2 cm<sup>-1,4</sup> (Figure 3F). The detection of such groups demonstrates the effective loading of the OL drug molecules within the EXK/CF composite as a carrier.

**2.2. Loading Properties and Mechanisms.** **2.2.1. Loading Properties.** **2.2.1.1. Effect of Time Intervals.** The effect of the studied loading intervals in detecting the saturation capacity of the EXK/CF composite as a drug carrier was evaluated considering the used EXK/CF dosage of 25 mg, the

volume of 250 mL, the OL concentration of 200 mg/L, and the temperature of 25 °C. The loading behavior of EXK/CF with time reflected a considerable enhancement for the OL drug on expanding the loading time intervals until a certain level, followed by slight or no changes in the loaded OL quantities, which reflected attainment of the saturation or the equilibration state for the carrier (Figure 4A). The loading

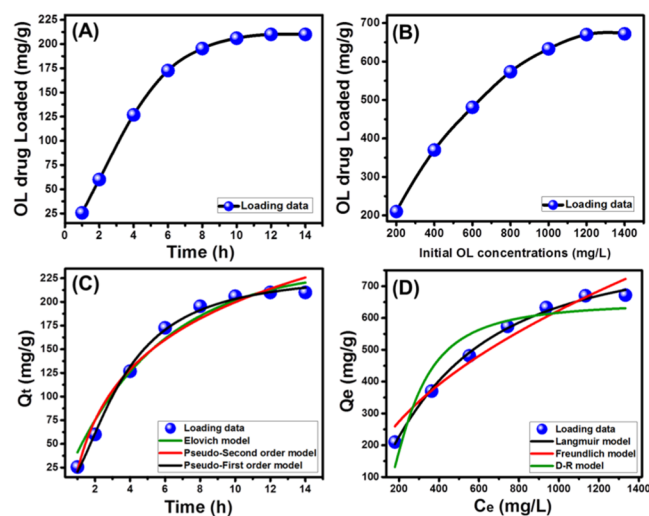


**Figure 4.** Loading capacities of the OL drug by EXK/CF with time (A) and using different OL concentrations (B); fitting of the loading results with different kinetic models (C) and with different isotherm models (D).

capacity at the equilibrium stage for the EXK/CF carrier is 210 mg/g detected after an equilibrium loading interval of 12 h (Figure 4A). The observed increment in the loaded quantities of the OL drug on expanding the addressed intervals was accompanied with a noticeable declination in the loading rates. Such behavior was because of the continuous occupation of the essential active loading sites in the EXK/CF composite with OL molecules with time, making the loading process limited by the remaining sites until reaching the full occupation.<sup>8</sup>

**2.2.1.2. Effect of OL Concentrations.** The loading behavior of EXK/CF at different concentrations of OL drug was investigated to determine its maximum capacity as a delivery system. The test was conducted considering the loading period of 14 h, the EXK/CF dosage of 25 mg, and the temperature of 25 °C. The observed results verified increment in the loading capacity on raising the investigated OL concentrations, which is of vital importance in controlling the loaded quantities of the drug (Figure 4B). The enhancement in the OL loading capacity continued until achieving a loading capacity of 670 mg/g at a tested concentration of 1200 mg/L, which can be categorized as the equilibrium concentration for the EXK/CF loading system. Such improvement in the OL loading capacities with testing higher concentrations of the OL drug was attributed to the expected increase in the driving forces of the present OL molecules, which promoted their adsorption by the EXK/CF active sites.<sup>12</sup>

The recognized OL maximum loading capacity and the possible control for the loaded quantity based on the loading factors reflected the suitability of the EXC/CF system to be used as a drug carrier with enhanced loading properties. Such excellent loading capacity might be related to the nature of the composite as a multifunctional hybrid structure of different

active functional groups, high surface reactivity, high surface area, and excellent adsorption properties. Other factors having a promising effect on increasing the loading capacity are related to the increase in the basal spacing between the kaolinite units, giving the structure high porosity, and the role of the intercalated reagents in providing new functional groups of high affinity for the organic molecules of the OL drug.<sup>13</sup>

### 2.2.2. Loading Kinetic and Equilibrium Properties.

**2.2.2.1. Kinetic Behavior.** The kinetic modeling for the OL loading reactions using EXK/CF as a carrier was studied using three models (the pseudo-first-order model, pseudo-second-order model, and Elovich model) (Figure 4C). The theoretical formulas of the addressed models are presented in their linear and nonlinear forms in Table S1. The fitting degree was evaluated based on the values of the determination coefficient as well as the chi-square ( $\chi^2$ ) (Figure 4C and Table 1).

**Table 1.** Theoretical Parameters of the Evaluated Kinetic and Equilibrium Models

	models	parameters	values
kinetic models	pseudo-first-order	$K_1$ (mg/min)	0.09
		$q_{e(\text{Cal})}$ (mg/g)	230.4
		$R^2$	0.98
		$\chi^2$	0.2
		$X^2$	1.3
	pseudo-second-order	$k_2$ (mg/min)	0.19
		$q_{e(\text{Cal})}$ (mg/g)	236.9
		$R^2$	0.97
		$\chi^2$	1.3
		$X^2$	1.45
Elovich	$\beta$ (g/mg)	0.013	
	$\alpha$ (mg/(g min))	101.8	
	$R^2$	0.95	
	$\chi^2$	1.45	
	$X^2$	1.45	
isotherm models	Langmuir	$q_{\text{max}}$ (mg/g)	704.4
		$b$ (L/mg)	$3.54 \times 10^{-4}$
		$R^2$	0.984
		$\chi^2$	1.83
		$X^2$	5.3
	Freundlich	$1/n$	0.51
		$k_F$	18.34
		$R^2$	0.95
		$\chi^2$	5.3
		$X^2$	5.3
D-R model	$\beta$ (mol <sup>2</sup> /kJ <sup>2</sup> )	0.0083	
	$q_m$ (mg/g)	649.2	
	$R^2$	0.88	
	$\chi^2$	4.03	
	$E$ (kJ/mol)	7.72	

The loading results show great agreement with both the pseudo-first-order assumption and the pseudo-second-order assumption. However, the estimated values of the determination coefficient ( $R^2$ ), as well as the chi-square ( $\chi^2$ ), reflected a higher fitting degree with the theoretical hypothesis of the pseudo-first-order model than the pseudo-second-order model (Figure 4C and Table 1). The previous results demonstrated the possible loading of the OL drug molecules by physical interaction with the essential active sites of the EXK/CF carrier. The observed significant fitness with the pseudo-second-order model reflected the operation of some chemical reactions during the loading process but as assistance mechanisms like surface complexation, electron exchange, and electron sharing reactions.<sup>11</sup> This conclusion was induced by the recognized considerable agreement between the loading results and the Elovich kinetic model that also suggested

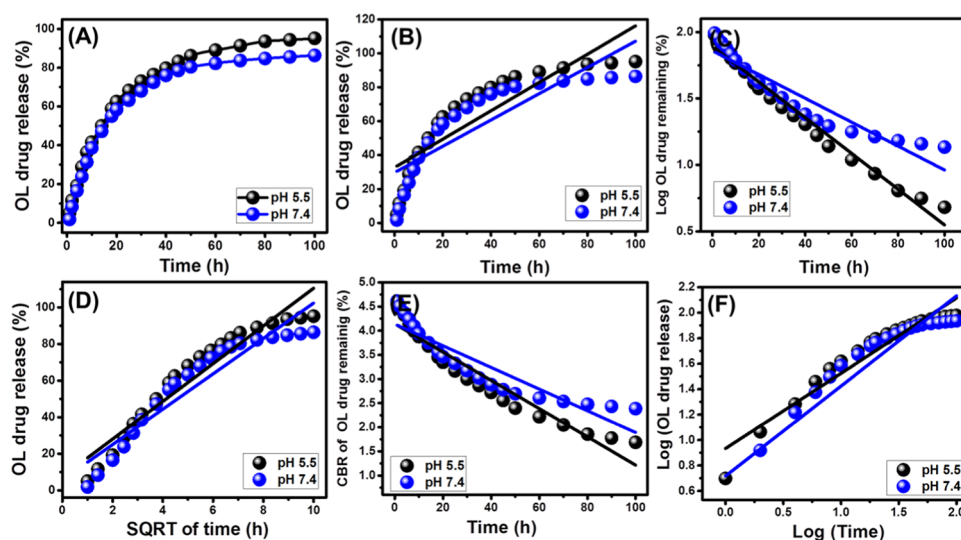


**Figure 5.** Release profiles of OL molecules from the EXK/CF carrier at pH 5.5 and pH 7.4 (A), fitting of the releasing results with the zero-order model (B), first-order model, (C) Higuchi model (D), Hixson–Crowell model (E), and Korsmeyer–Peppas model (F).

energetic heterogeneous properties of the surface of the EXK/CF composite during the loading reactions of the OL drug.

**2.2.2.2. Equilibrium Modeling.** The equilibrium properties of the studied OL loading reactions using the synthetic EXK/CF composite as a carrier were inspected considering the nonlinear fitting degree with the three commonly used models of Langmuir, Freundlich, and Dubinin–Radushkevich (Figure 4D and Table 1). The representative equations of these models in their linear and nonlinear forms both are listed in Table S1. The fitting degree based on the values of the determination coefficient ( $R^2$ ), as well as the chi-square ( $\chi^2$ ), reflected higher agreement for the loading behavior of the OL drug with the Langmuir model than the other models (Table 1 and Figure 4D). This demonstrated the loading of the OL drug molecules by the synthetic EXK/CF carrier in a homogeneous and a monolayer form. As a theoretical factor for the excellent fitting with the Langmuir model, the theoretical maximum loading capacity of the OL drug by the EXK/CF composite is 704.4 mg/g.

Considering the effective role of the theoretical factors of the Dubinin–Radushkevich model (D–R) in determining the type of control mechanism for loading (chemical or physical), the Gaussian energy was estimated and is presented in Table 1<sup>22</sup>. The obtained value for the loaded OL drug molecules is 7.72 kJ/mol, suggesting physisorption mechanisms for the loading of the drug molecules into the EXK/CF composite.<sup>23</sup>

The FT-IR spectra of the composite after its loading with the OL molecules reflected a strong reduction of the OH absorption bands of exfoliated kaolinite especially those of siloxane groups (Si–OH), which are the most active groups in the kaolinite structure. This proved the adsorption of the OL molecules by these active groups, forming types of hydrogen bonds as the essential loading mechanism. Additionally, this was observed for the –O–H, –C–H, and –C–O–C groups for the integrated cellulose, demonstrating their role as essential sites for the loaded OL molecules.<sup>13</sup>

**2.3. In Vitro Release Profiles.** The inspected curves for the release of OL drug molecules from the EXK/CF carrier in the phosphate buffer solution (pH 7.4) or the acetate buffer solution (pH 5.5) demonstrated the existence of two obvious segments related to different releasing rates of the loaded drug

(Figure 5A). The first segment showed an abrupt or very fast releasing rate that might be related to the predicted diffusion of the OL drug as adsorbed molecules from the external active sites of the EXK/CF composite into the buffer solutions as they are having weak hydrogen bonds with such functional groups.<sup>8</sup> The second segment was associated with very limited variation in the observed releasing rate, showing a recognizable state of equilibration and the maximum releasing capacity for the loaded drug (Figure 5A). The release in this stage was limited because of the slow diffusion of the entrapped drug molecules within the cellulose matrix or formation of a complex with the essential active functional groups<sup>20,24</sup> as reported by FT-IR analysis. Additionally, the predicted entrapping of the OL drug as intercalated molecules between the kaolinite units had an effective role in reducing the diffusion rates of the drug into the buffer solutions.

The studied release profile of EXK/CF as an advanced carrier for the OL drug was evaluated for about 100 h (Figure 5A). The presented results demonstrated a promising release profile with very continuous and slow properties. This resulted in incomplete diffusion of the OL loaded quantities in the phosphate solution (pH 7.4) or the acetate solution (pH 5.5) used (Figure 5A). The determined maximum percentages for the release of the OL drug after 100 h are 86.4 and 95.2% in the studied phosphate buffer and acetate buffer solutions, respectively (Figure 5). The reported slow release properties of the synthetic EXK/CF as a carrier for the OL drug might be ascribed to the expected formation of strong hydrogen bonds between the active functional groups of the drug and the siloxane groups of exfoliated kaolinite that became highly reactive after the exfoliation processes.<sup>25</sup> It was reported that the release profiles that exhibit continuous and slow diffusion properties are of promising effect during the treatment of the cancer cell. This was related to the constant exposure of the cancer cells to the released drug molecules, inducing the inhibition of the proliferation of the target cancer cells.<sup>5</sup>

**2.4. Release Kinetic Studies.** The predicted mechanisms that might control the release of the molecules from the structure of the EXK/CF composite were studied considering the theoretical assumption of different types of release kinetic models. The addressed models in the study are the zero-order

kinetic model, first-order kinetic model, Higuchi kinetic model, Hixson–Crowell kinetic model, and Korsmeyer–Peppas kinetic model. The fitting processes were conducted by the linear regression fitness, and the corresponding theoretical equations (eqs 1–5) for the previously mentioned models are as follows<sup>26</sup>

$$W_t - W_0 = K_0 \cdot t \quad (1)$$

$$\ln (W_\infty/W_t) = K_1 \cdot t \quad (2)$$

$$W_t = K_H t^{1/2} \quad (3)$$

$$W_0^{1/3} - W_t^{1/3} = K_{HC} t \quad (4)$$

$$W_t/W_\infty = K_p t^n \quad (5)$$

The assumption of the zero-order kinetic model suggested that the diffusion of the loaded drug molecules occurs at a constant rate and that the releasing behavior is not affected by the concentration of the studied drug.<sup>27</sup> On the other hand, the first-order kinetic model was used to evaluate the releasing systems that were strongly controlled by the loaded quantities of the studied drug.<sup>20</sup> As for the Higuchi kinetic model, it is commonly used to study the drug carrier systems in which the release of the loaded drug occurs mainly by the dissolution and diffusion mechanism.<sup>20</sup> This model suggested six limitations predicted for the releasing systems that follow its hypothesis: (1) the loaded molecules are of higher concentration than their releasing rate, (2) there is one direction for the diffused drug molecules from the carrier, (3) the loaded drug has a diameter less than the reported value for the thickness of the carrier, (4) the releasing rates are not controlled by the swelling index or the solubility of any existing polymer as a structural component, (5) the loaded drug shows a constant diffusion rate, and (6) the drug molecules exhibit significant sink properties during their release from the carrier.<sup>27,28</sup>

The Hixson–Crowell kinetic model assumes the diffusion of the studied drug molecules in the form of parallel planes with continuous declination in the dimension of the addressed carrier, which reflects strong dependence on the surface area as well as the diameter of the selected carrier. Generally, this model suggests controlling the releasing behavior by the erosion mechanism.<sup>8</sup> The Korsmeyer–Peppas kinetic model was categorized as the best kinetic model that can explain the release profiles of polymer-based drug carriers either by the diffusion mechanism or by the erosion mechanism and sometimes a combination of them.<sup>20</sup>

The degree by which the obtained results fitted with the presented models was evaluated based on the reported values of the determination coefficient ( $R^2$ ) (Figure 5B and Table 2).

**Table 2. Determined Values of the Determination Coefficient Which Were Obtained for Linear Regression Fitting of the Releasing Results with the Kinetic Models**

models	determination coefficient ( $R^2$ )	
	pH 5.5	pH 7.4
zero-order model	0.75	0.71
first-order model	0.97	0.88
Higuchi model	0.91	0.89
Hixson–Crowell model	0.91	0.83
Korsmeyer–Peppas model	0.92	0.86

The releasing behavior of OL from the EXK/CF composite is in poor agreement with the investigated zero-order model as compared to the first-order model (Figure 5C and Table 2) or the other assessed models, reflecting the strong effect of the loaded quantity of OL in controlling the release profile in the studied buffer solutions (the acetate solution or the phosphate solution).

The results demonstrated strong agreement with the assumption of the Higuchi model, suggesting a significant effect of the diffusion mechanism during the release of OL molecules from the EXK/CF composite as a carrier (Figure 5D and Table 2). This was observed also for the fitting results with the Hixson–Crowell model, suggesting a principal role of the erosion mechanism in controlling the release behavior (Figure 5E and Table 2). The observed high agreement with the Higuchi model as well as the Hixson–Crowell model reflected the operation of diffusion and erosion mechanisms during the release of the OL drug from the synthetic EXK/CF composite with possible dominance of the erosion model in the phosphate buffer solution (pH 7.4).

Finally, the releasing data is in significant agreement with the addressed Korsmeyer–Peppas model, and the estimated values of the diffusion exponent ( $n$ ) of the studied acetate and phosphate solutions are 0.59 and 0.70, respectively (Figure 5F). These values are related to non-Fickian transport behaviors that involve the erosion mechanism as well as the diffusion mechanism during the release of OL from the EXK/CF composite.<sup>8</sup>

**2.5. Cytotoxicity Properties.** The cytotoxicity properties of the synthetic EXK/CF composite as a pure phase and OL-loaded EXK/CF were determined for both the normal cell (CCD-18Co) and the cancer cell (HCT116) based on the results of MTT assay tests (Figure 6). The EXK/CF concentrations for the investigation of its cytotoxic effect on the studied normal cell (CCD-18Co) were selected within an

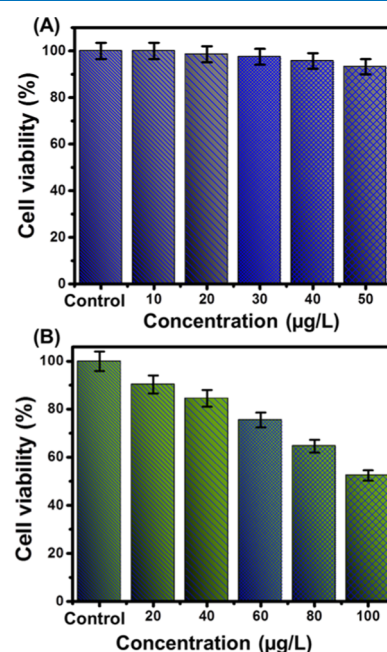


**Figure 6.** Cytotoxicity of EXK/CF toward the human colorectal fibroblast cell (CCD-18Co) (A) and viability of human colorectal cancer cell (HCT116) after treating it with EXK/CF loaded with the OL drug (B).

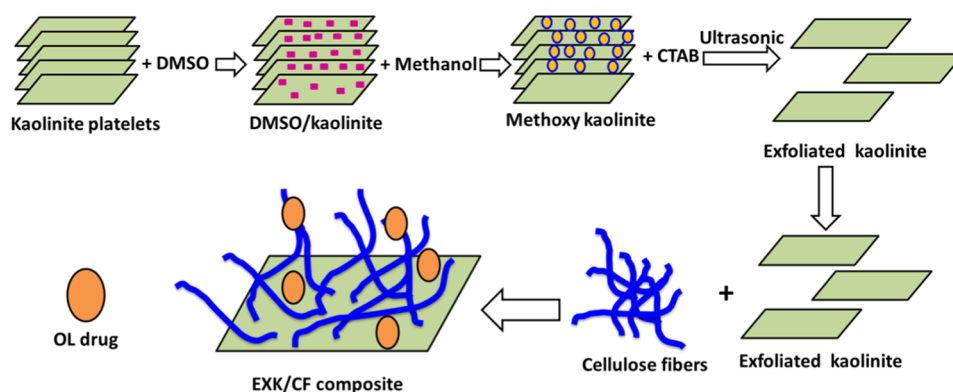


**Figure 7.** Schematic diagram for the synthesis of the EXK/CF composite and its loading with the OL drug.

experimental range from 10 to 50  $\mu\text{g/L}$ . The reported values of the cell viability demonstrated promising safety and biocompatibility properties of the EXK/CF composite as a drug carrier, achieving 93.24% cell viability for the highest applied concentration in the test (50  $\mu\text{g/L}$ ) (Figure 6A). Regarding the tests performed to investigate the toxicity effect of OL-loaded EXK/CF on the cancer cell (HCT116), the results proved higher toxic effects of the OL-loaded EXK/CF composite on the colorectal cancer cell than those of the OL drug molecules in free form without a carrier (Figure 6B). The cell viability for the cancer cell (HCT116) that was obtained for the OL drug in its free form was 77%, while the obtained value for OL-loaded EXK/CF reached 31.4%. Such values verified considerable enhancement in the efficiency and the safety properties of the oxaliplatin drug for chemotherapy of colorectal cancer after loading it into the EXK/CF composite as an advanced delivery system.

### 3. CONCLUSIONS

Exfoliated kaolinite single sheets were used successfully in the synthesis of the composite with cellulose fibers (EXK/CF) of 104  $\text{m}^2/\text{g}$  surface area and were used as a carrier for the oxaliplatin (OL) drug. The EXK/CF composite achieved an experimental loading capacity of 670  $\text{mg/g}$ , and the loading behavior followed the theoretical hypothesis of the pseudo-first-order kinetic model and the Langmuir equilibrium model with a loading energy of 7.7  $\text{kJ/mol}$ . The release profile continued for 100 h, and the maximum percentages in the phosphate and acetate buffers are 86.4 and 95.2%, respectively. The kinetic modeling and the diffusion exponent suggested a combination of the erosion and diffusion mechanisms during the release of the OL drug. The cytotoxicity studies reflected a highly safe effect on the normal colorectal cells (CCD-18Co) with 93.24% as the maximum cell viability and highly toxic effect on the colorectal cancer cell (HCT116) with 31.4% cell viability.

### 4. EXPERIMENTAL WORK

**4.1. Materials.** The kaolinite powder was obtained from the Central Metallurgical Research & Development Institute, Egypt, for the exfoliation process. Cetyltrimethylammonium bromide (CTAB), methanol, and dimethyl sulfoxide (DMSO) of high purity grades were obtained from Sigma-Aldrich, Egypt, and applied as exfoliation reagents. Crystalline cellulose fibers and the oxaliplatin (OL) drug of analytical grades were used in the preparation of the composite and in the evaluation of the loading and releasing properties for the drug.

**4.2. Exfoliation of Kaolinite (EXK).** The exfoliated kaolinite was obtained as a transitional state for the scrolling of kaolinite into nanotubes according to Abukhadra and Allah.<sup>13</sup> The accomplished procedures involved, first, the dispersion of kaolinite powder (15 g) within the diluted solution of DMSO (50 mL (10% distilled water + 80% DMSO)) followed by stirring for 2 h as an essential stage to break the existing hydrogen bonds between the structural kaolinite sheets. The product obtained during this stage was kaolinite sheets intercalated with DMSO. This product was washed five times using methanol, each run consumed 20 min to replace the DMSO molecules by methanol molecules, forming methoxy kaolinite. Then, the methoxy kaolinite was added to the surfactant solution (CTAB) (50 mL) and stirred for 48 h to increase the expansion between the layers and exfoliate them from each other (Figure 7). Then, the EXK supernatant was separated, washed extensively with ethanol as well as distilled water, and dried at 60  $^{\circ}\text{C}$  for 12 h to be used in the next synthesis step.

**4.3. Synthesis of the Exfoliated Kaolinite/Cellulose Fiber (EXK/CF) Composite.** The integration between the exfoliated kaolinite sheets and the cellulose fibers was accomplished using 6 g of the prepared EXK particles. The EXK fractions were mixed homogeneously with 30 mL of distilled water and stirred for 120 min at a speed adjusted to 500 rpm, and then, the dispersion processes were induced using a sonication source with the power adjusted to 240 W for another 120 min. After this step, the EXK supernatant was mixed with 30 mL of a solution containing 3 g of dispersed cellulose and stirred for 24 h at a speed of 500 rpm. Then, the whole mixture was treated with sonication irradiation at a permanent power of 240 W for 4 h to induce integration between the EXK fractions and cellulose as biopolymers. Finally, the prepared exfoliated kaolinite/cellulose fibers (EXK/CF) composite was dried for 24 h at 65  $^{\circ}\text{C}$  (Figure 7).

**4.4. Characterization Techniques.** The crystalline properties were studied using a PANalytical X-ray diffractometer (Empyrean). The effect of the combination process on the essential chemical functional groups was addressed using Bruker FT-IR spectrometer (Vertex 70). Moreover, the external morphologies and the internal structures were evaluated using a scanning electron microscope (Gemini, Zeiss-Ultra 55) and a transmission electron microscope (JEOL-JEM2100), respectively.

**4.5. Loading Properties of the Oxaliplatin Drug.** The loading behavior, capacity, and the controlling mechanism of the EXK/CF composite for the oxaliplatin drug were

investigated considering the loading behavior for different time intervals (1–14 h) and different OL concentrations in the prepared aqueous solutions (200–1400 mg/L). Homogenization between the carrier fractions and the drug-bearing solutions was performed using a vortex rotator, and after each performed test, the solution was separated using a centrifuge. The OL residual concentration was determined by an ultraviolet (UV) spectrophotometer after adjusting the  $\lambda_{\max}$  to 209 nm. The loading capacities were calculated from eq 6<sup>12</sup>

$$\text{loaded drug (mg/g)} = \frac{(\text{initial concentration} - \text{residual concentration}) \times \text{solvent volume}}{\text{carrier weight}} \quad (6)$$

**4.6. In Vitro Release Profiles.** The in vitro release profile of EXK/CF after its loading with the OL drug was studied using two types of buffer solutions: saline phosphate buffer (pH 7.4) and saline acetate buffer (pH 5.5) at an adjusted temperature of 37.5 °C. The release profile was followed by inspection of regular samples from the solutions (3 mL) after regular releasing intervals to detect the diffused OL molecules using the UV–vis spectrophotometer at an adjusted  $\lambda_{\max}$  of 209 nm. The percentages of the released OL molecules were calculated using eq 7<sup>20</sup>

$$\text{drug release (\%)} = \frac{\text{the amount of released OL drug}}{\text{amount of loaded OL}} \times 100 \quad (7)$$

**4.7. In Vitro Cytotoxicity.** The cytotoxic effect of EXK/CF before and after its loading with the OL molecules was inspected on the normal human colorectal fibroblast cell (CCD-18Co) and the human colorectal cancer cell (HCT116). The cell lines were obtained from the American Type Culture Collection (ATCC, Rockville, MD), and all of the tests were performed in the Regional Center for Mycology & Biotechnology, Al-Azhar University, Egypt. The tested normal cell line and cancer cell line were grown in Dulbecco's modified Eagle's medium (DMEM) and RPMI1640 medium, respectively. The used growing media were supplemented with 10% fetal bovine serum and 1% penicillin/streptomycin and kept in an incubator at a temperature adjusted to 37 °C in the presence of a CO<sub>2</sub> atmosphere (5%). The cytotoxic effect on the studied cells was determined by the MMT assay. The studied cells were seeded in 96-well plates, incubated for 24 h (as the growing period), then mixed with different concentrations of the synthetic EXK/CF composite and OL-loaded EXK/CF, and then left in the incubator for 48 h. Then, the incorporated media were removed effectively, and the studied cells were treated with the MTT solution (100  $\mu$ L; 1 mg/mL). After the addition of the MTT solution, the cells were kept in the incubator again for another 2 h under humid conditions at 37 °C temperature and a 5% CO<sub>2</sub> atmosphere. After this step, the incorporated MTT solutions were completely removed and treated using 100  $\mu$ L of DMSO as a process required to dissolve the formazan crystals that were formed during the test. Finally, the absorbance of the samples was measured using a microplate reader at 570 nm.

## ■ ASSOCIATED CONTENT

### Supporting Information

The Supporting Information is available free of charge at <https://pubs.acs.org/doi/10.1021/acsomega.0c02529>.

Representative equations of the studied kinetic and isotherm models in Table S1 (PDF)

## ■ AUTHOR INFORMATION

### Corresponding Author

**Mostafa R. Abukhadra** – *Geology Department, Faculty of Science and Materials Technologies and their Applications Lab, Geology Department, Faculty of Science, Beni-Suef University, Beni Suef 62511, Egypt; [orcid.org/0000-0001-5404-7996](https://orcid.org/0000-0001-5404-7996); Email: [Abukhadra89@Science.bsu.edu.eg](mailto:Abukhadra89@Science.bsu.edu.eg)*

### Authors

**Lijun Tian** – *Deputy Chief Physician, Shanxi Provincial People's Hospital, Taiyuan 030012, Shanxi Province, China*

**Aya S. Mohamed** – *Materials Technologies and their Applications Lab, Geology Department, Faculty of Science and Department of Environment and Industrial Development, Faculty of Postgraduate Studies for Advanced Sciences, Beni-Suef University, Beni Suef 62511, Egypt*

**Ahmed Nadeem** – *Department of Pharmacology & Toxicology, College of Pharmacy, King Saud University, Riyadh 11451, Saudi Arabia*

**Sheikh F. Ahmad** – *Department of Pharmacology & Toxicology, College of Pharmacy, King Saud University, Riyadh 11451, Saudi Arabia*

**Khalid E. Ibrahim** – *Department of Zoology, College of Science, King Saud University, Riyadh 11451, Saudi Arabia*

Complete contact information is available at: <https://pubs.acs.org/10.1021/acsomega.0c02529>

### Author Contributions

This article was written through the contributions of all authors. All authors have given approval to the final version of the manuscript.

### Notes

The authors declare no competing financial interest. Further study will be conducted to investigate the behavior of the EXK/CF composite as a carrier for the oxaliplatin drug in the body of animals through in vivo studies to evaluate the realistic role of the carrier in the efficiency of the oxaliplatin drug.

## ■ ACKNOWLEDGMENTS

The authors acknowledge and extend their appreciation to the Researchers Supporting Program with Project No. RSP-2019-124, King Saud University, Riyadh, Saudi Arabia, for funding this study.

## ■ REFERENCES

- (1) Ren, Y.; Li, X.; Han, B.; Zhao, N.; Mu, M.; Wang, C.; Du, Y.; Wang, Y.; Tong, A.; Liu, Y.; Zhou, L.; You, C.; Guo, G. Improved anti-colorectal carcinomatosis effect of tannic acid co-loaded with oxaliplatin in nanoparticles encapsulated in thermosensitive hydrogel. *Eur. J. Pharm. Sci.* **2019**, *128*, 279–289.
- (2) Ullah, K.; Khan, S. A.; Murtaza, G.; Sohial, M.; Manan, A.; Afzal, A. Gelatin-based hydrogels as potential biomaterials for colonic delivery of oxaliplatin. *Int. J. Pharm.* **2019**, *556*, 236–245.
- (3) Jain, A.; Jian, S. K.; Ganesh, N.; Brave, J.; Beg, A. M. Design and development of ligand-appended polysaccharidic nanoparticles for the delivery of oxaliplatin in colorectal cancer. *Nanomedicine* **2010**, *6*, 179–190.
- (4) Liang, C.; Wang, H.; Zhang, M.; Cheng, W.; Li, Z.; Nie, J.; Liu, G.; Lian, D.; Xie, Z.; Huang, L.; Zeng, X. Self-controlled release of Oxaliplatin prodrug from d- $\alpha$ -tocopheryl polyethylene glycol 1000 succinate (TPGS) functionalized mesoporous silica nanoparticles for cancer therapy. *J. Colloid Interface Sci.* **2018**, *525*, 1–10.

- (5) Sundaramoorthy, P.; Ramasamy, T.; Mishra, S. K.; Jeong, K. Y.; Yong, C. S.; Kim, J. O.; Kim, H. M. Engineering of caveolae-specific self-micellizing anticancer lipid nanoparticles to enhance the chemotherapeutic efficacy of oxaliplatin in colorectal cancer cells. *Acta Biomater.* **2016**, *42*, 220–231.
- (6) Vatanparast, M.; Shariatnia, Z. AlN and AlP doped graphene quantum dots as novel drug delivery systems for 5-fluorouracil drug: theoretical studies. *J. Fluorine Chem.* **2018**, *211*, 81–93.
- (7) Chandran, S. P.; Natarajan, S. B.; Chandraseharan, S.; Shahimi, M. S. B. M. Nano drug delivery strategy of 5-fluorouracil for the treatment of colorectal cancer. *J. Cancer Res. Pract.* **2017**, *4*, 45–48.
- (8) Abukhadra, M. R.; Refay, N. M.; El-Sherbeeny, A. M.; Mostafa, A. M.; Elmeligy, M. A. Facile synthesis of bentonite/biopolymer composites as low-cost carriers for 5-fluorouracil drug; equilibrium studies and pharmacokinetic behavior. *Int. J. Biol. Macromol.* **2019**, *141*, 721–731.
- (9) Shad, P. M.; Karizi, S. Z.; Javan, R. S.; Mirzaie, A.; Noorbazargan, H.; Akbarzadeh, I.; Rezaie, H. Folate conjugated hyaluronic acid coated alginate nanogels encapsulated oxaliplatin enhance antitumor and apoptosis efficacy on colorectal cancer cells (HT29 cell line). *Toxicol. In Vitro* **2020**, *65*, No. 104756.
- (10) He, H.; Xiao, H.; Kuang, H.; Xie, Z.; Chen, X.; Jing, X.; Huang, Y. Synthesis of mesoporous silica nanoparticle–oxaliplatin conjugates for improved anticancer drug delivery. *Colloids Surf., B* **2014**, *117*, 75–81.
- (11) Shaban, M.; Sayed, M. I.; Shahien, M. G.; Abukhadra, M. R.; Ahmed, Z. M. Adsorption behavior of inorganic-and organic-modified kaolinite for Congo red dye from water, kinetic modeling, and equilibrium studies. *J. Sol-Gel Sci. Technol.* **2018**, *87*, 427–441.
- (12) Dardir, F. M.; Mohamed, A. S.; Abukhadra, M. R.; Ahmed, E. A.; Soliman, M. F. Cosmetic and pharmaceutical qualifications of Egyptian bentonite and its suitability as drug carrier for Praziquantel drug. *Eur. J. Pharm. Sci.* **2018**, *115*, 320–329.
- (13) Abukhadra, M. R.; Allah, A. F. Synthesis and characterization of kaolinite nanotubes (KNTs) as a novel carrier for 5-fluorouracil of high encapsulation properties and controlled release. *Inorg. Chem. Commun.* **2019**, *103*, 30–36.
- (14) Tan, D.; Yuan, P.; Annabi-Bergaya, F.; Liu, D.; He, H. High-capacity loading of 5-fluorouracil on the methoxy-modified kaolinite. *Appl. Clay Sci.* **2014**, *100*, 60–65.
- (15) Ma, J.; Huang, D.; Zhang, W.; Zou, J.; Kong, Y.; Zhu, J.; Komarneni, S. Nanocomposite of exfoliated bentonite/g-C<sub>3</sub>N<sub>4</sub>/Ag<sub>3</sub>PO<sub>4</sub> for enhanced visible-light photocatalytic decomposition of Rhodamine B. *Chemosphere* **2016**, *162*, 269–276.
- (16) Abukhadra, M. R.; Bakry, B. M.; Adlii, A.; Yakout, S. M.; El-Zaidy, M. E. Facile conversion of kaolinite into clay nanotubes (KNTs) of enhanced adsorption properties for toxic heavy metals (Zn<sup>2+</sup>, Cd<sup>2+</sup>, Pb<sup>2+</sup>, and Cr<sup>6+</sup>) from water. *J. Hazard. Mater.* **2019**, *374*, 296–308.
- (17) Putro, J. N.; Santoso, S. P.; Ismadji, S.; Ju, Y. H. Investigation of heavy metal adsorption in binary system by nanocrystalline cellulose–bentonite nanocomposite: improvement on extended Langmuir isotherm model. *Microporous Mesoporous Mater.* **2017**, *246*, 166–177.
- (18) Fakhri, A.; Tahami, S.; Nejad, P. A. Preparation and characterization of Fe<sub>3</sub>O<sub>4</sub>-Ag<sub>2</sub>O quantum dots decorated cellulose nanofibers as a carrier of anticancer drugs for skin cancer. *J. Photochem. Photobiol., B* **2017**, *175*, 83–88.
- (19) Pooresmaeil, M.; Javanbakht, S.; Nia, S. B.; Namazi, H. Carboxymethyl cellulose/mesoporous magnetic graphene oxide as a safe and sustained ibuprofen delivery bio-system: Synthesis, characterization, and study of drug release kinetic. *Colloids Surf., A* **2020**, *594*, No. 124662.
- (20) El-Zeiny, H. M.; Abukhadra, M. R.; Sayed, O. M.; Ahmed, S. A.; Osman, A. H. Insight into novel  $\beta$ -cyclodextrin-grafted-poly (N-vinylcaprolactam) nanogel structures as advanced carriers for 5-fluorouracil: Equilibrium behavior and pharmacokinetic modeling. *Colloids Surf., A* **2020**, *586*, No. 124197.
- (21) Chen, W.; He, H.; Zhu, H.; Cheng, M.; Li, Y.; Wang, S. Thermo-responsive cellulose-based material with switchable wettability for controllable oil/water separation. *Polymers* **2018**, *10*, No. 592.
- (22) Rajabi, M.; Mirzab, B.; Mahanpoorc, K.; Mirjalilid, M.; Najafi, F.; Moradif, O.; Sadeq, H.; Shahryari-ghoshekandi, R.; Asif, M.; Tyagi, I.; Agarwal, S.; Gupta, V. K. Adsorption of malachite green from aqueous solution by carboxylate group functionalized multi-walled carbon nanotubes: Determination of equilibrium and kinetics parameters. *J. Ind. Eng. Chem.* **2016**, *34*, 130–138.
- (23) Abukhadra, M. R.; Mostafa, M. Effective decontamination of phosphate and ammonium utilizing novel muscovite/phillipsite composite; equilibrium investigation and realistic application. *Sci. Total Environ.* **2019**, *667*, 101–111.
- (24) Goscianska, J.; Olejnik, A.; Nowak, I.; Marciniak, M.; Pietrzak, R. Ordered mesoporous silica modified with lanthanum for ibuprofen loading and release behavior. *Eur. J. Pharm. Biopharm.* **2015**, *94*, 550–558.
- (25) Rehman, F.; Ahmed, K.; Rahim, A.; Muhammad, N.; Tariq, S.; Azhar, U.; Khan, A. J.; us Sama, Z.; Volpe, pL.; Airoidi, C. Organobridged silsesquioxane incorporated mesoporous silica as a carrier for the controlled delivery of ibuprofen and fluorouracil. *J. Mol. Liq.* **2018**, *258*, 319–326.
- (26) Arifin, D. Y.; Lee, L. Y.; Wang, C.-H. Mathematical modeling and simulation of drug release from microspheres: implications to drug delivery systems. *Adv. Drug Delivery Rev.* **2006**, *58*, 1274–1325.
- (27) Gouda, R.; Baishya, H.; Qing, Z. Application of Mathematical Models in Drug Release Kinetics of Carbidopa and Levodopa ER Tablets. *J. Dev. Drugs* **2017**, *62* DOI: 10.4172/2329-6631.1000171.
- (28) Ramteke, K. H.; Dighe, P. A.; Kharat, A. R.; Patil, S. V. Mathematical models of drug dissolution: a review. *Sch. Acad. J. Pharm.* **2014**, *3*, 388–396.